UNIVERSITY OF LEEDS

This is a repository copy of *Multi-view Stereophotogrammetry for Post-mastectomy Breast Reconstruction*.

White Rose Research Online URL for this paper:
http://eprints.whiterose.ac.uk/87691/

Version: Accepted Version

Article:
Ju, X, Henseler, H, Peng, MJ et al. (3 more authors) (2016) Multi-view Stereophotogrammetry for Post-mastectomy Breast Reconstruction. Medical and Biological Engineering and Computing, 54 (2). pp. 475-484. ISSN 0140-0118

https://doi.org/10.1007/s11517-015-1334-3

Reuse
Unless indicated otherwise, fulltext items are protected by copyright with all rights reserved. The copyright exception in section 29 of the Copyright, Designs and Patents Act 1988 allows the making of a single copy solely for the purpose of non-commercial research or private study within the limits of fair dealing. The publisher or other rights-holder may allow further reproduction and re-use of this version - refer to the White Rose Research Online record for this item. Where records identify the publisher as the copyright holder, users can verify any specific terms of use on the publisher's website.

Takedown
If you consider content in White Rose Research Online to be in breach of UK law, please notify us by emailing eprints@whiterose.ac.uk including the URL of the record and the reason for the withdrawal request.

White Rose university consortium
Universities of Leeds, Sheffield & York

eprints@whiterose.ac.uk
https://eprints.whiterose.ac.uk/

Manuscript
Click here to download Manuscript: MBEC_2014.tex
Click here to view linked References

Med Biol Eng Compu manuscript No.
(will be inserted by the editor)

Multi-view Stereophotogrammetry for Post-mastectomy Breast Reconstruction

Xiangyang Ju · Helga Henseler · Matthew Jian-qiao Peng · Balvinder S Khambay · Arup K Ray · Ashraf F Ayoub

Received: date / Accepted: date

Abstract A multi-view three dimensional stereophotogrammetry system was developed to capture 3D shape of breasts for breast cancer patients. The patients had received immediate unilateral breast reconstruction after mastectomy by the extended latissimus dorsi flap and without contra-lateral surgery. In order to capture the whole breast shape including the infra mammary fold, the patients were introduced to the imaging room and leaned over the imaging rig to open up the infra mammary fold and to expose the entire area of each breast. The imaging system consisted of eight high-resolution (4504×3000 pixels) digital cameras and four flash units. The cameras were arranged in four stereo pairs from four different view angles to cover the whole surface of the breasts. The system calibration was carried out ahead of every capture

X. Ju
Medical Devices Unit, Southern General Hospital, Glasgow G51 4TF, UK.
Tel.: +44-141-2119737
E-mail: xiangyang.ju@glasgow.ac.uk

H. Henseler
Medizinische Hochschule Hannover (Hannover Medical School), Abteilung fr Plastische-, Hand- und Wiederherstellungschirurgie (Department of Plastic-, Hand- and Reconstructive Surgery) Carl-Neuberg-Strae 1, 30625 Hannover, Germany.

J. Peng
Dept. of Joint Surgery, First Affiliated Hospital of Guangzhou Medical University. Guangzhou Research Institute of Computational Orthopedics at Joint Implantation Key Laboratory of Guangdong Province, China.

B. Khambay
Pediatric Dentistry and Orthodontics, Faculty of Dentistry. The University of Hong Kong, Hong Kong.

A. Ray
Canniesburn Plastic Surgery Unit Glasgow, Glasgow Royal Infirmary, 84 Castle Street, Glasgow G4 0SF, UK.

A. Ayoub
Glasgow University MVLS college, Medical Faculty, Dental Hospital and School, 378 Sauchiehall Street, Glasgow G2 3JZ, UK.

session and the stereo images were matched to generate four range images to be integrated using an elastic model proposed. A watertight breast mesh model was reconstructed to measure the volume of the breast captured. The accuracy of using the developed multi-view stereophotogrammetry system for breast volume measurement was 11.12cc with SEM 7.74cc, comparing to the measurements of the water displacement method. It was concluded that the 3D stereophotogrammetry image system developed was more reliable than the method of water displacement.

Keywords Breast Reconstruction · Multi-view Stereo Photogrammetry · Range Image Integration · 3D Modelling

1 Introduction

Breast cancer accounts for nearly a quarter of all cancer cases amongst women worldwide and for 32% of the cancer burden in the UK for women. Bilateral mastectomy is increasingly being used as a risk reduction measure for the carriers of the breast cancer gene who have a high risk of developing breast cancer; and as a planned management strategy for unilateral cancer [1]. Current breast cancer treatment encompasses not only surgical removal of the tumor and medical adjuvant and neo-adjuvant therapies, but also an increasing emphasis lies on improving of a woman's quality of life [2]. Breast reconstruction plays an important role to restore breast symmetry following partial and total mastectomy procedures that result in abnormal volume, shape, and contours of breast with the aim of creating aesthetically pleasing and symmetrical breasts [3]. The conduct of breast reconstruction procedures currently remains largely subjective and is based on physical examination and visual-estimates of breast size, shape and symmetry. The plastic surgeons have difficulties to objectively assess breast volumes and shape, that may result in suboptimal outcomes [4, 5]. The field of reconstructive breast surgery would benefit from a practical method for objectively assessing breast volume. Precise measurement of breast volume could facilitate reconstructive procedures and help in surgical planning.

For breast volume measurement, previously anthropomorphic measurements [6]; water displacement [7,8] and plaster casting [9] were used, but these measurements were time intensive, and were intrusive for patients. Three-dimensional imaging techniques, such as structured light projections [10, 11], 3D laser scanning [4, 12, 13, 14] and 3D stereo photogrammetry imaging [2, 3, 15, 16] have been applied on patients' breast measurement that enable a surgeon to obtain quantitative breast measurements [17]; to make volumetric calculations and to visually and quantitatively assess reconstructed breasts. 3D X-ray imaging [18] was applied on 3D reconstruction of spine [19, 20], but it was radioactive and captured shapes only. 3D stereophotogrammetry imaging has advantages of fast image acquisition and photographic texture without radiation. The photographic texture provides the details of breast surface texture for identifying anatomical locations and for surgical planning. In most

of these studies reported, the patients were standing and the breast shapes were captured with a single view angle. However it was difficult to define the boundaries, to display infra mammary folds in the large breasts and also it was not possible to capture the whole breast surface from a single view angle. The captured breast shapes presented with a lack of data around the infra mammary fold. The infra mammary fold was visualized as holes in the images that led to poor agreement between the assessments made directly on the patients [2]. Hence multi-view stereo imaging photogrammetry was applied in order to capture the entire area of each breast.

2 Methods

A multi-view photogrammetry imaging system has been applied in the presented study to capture the entire breast surfaces. It is capable to capture multi-view stereo images simultaneously in less than $1ms$. The basic principle behind photogrammetric measurements is fairly straight forward, given two images of an object taken from different view angles, it is possible, using triangulation, to determine the original three-dimensional location of the object from its corresponding images. This is similar to the human vision in which the depth perceptions are interpreted from the disparities between the images in the left and right eyes. There are a few crucial steps to obtain the three-dimensional metrical shape of the object from their stereo images. The first is to determine automatically and accurately the point-wise correspondences between the stereo images. Having established the correspondence between stereo image points, a system can use triangulation to calculate the location of the object in 3D space. However this requires the information of the positions and orientations of the cameras, the focal lengths of the lens and the lens distortions, the image centers, the sensor element size and the image aspect ratio. These parameters can be determined by a process of calibration [21,22,23]. Multi-view stereo image pairs are necessary to cover the entire breast surface due to the object self-occlusion. Further, breast range images recovered from individual stereo image pairs have to be aligned/registered and integrated into a single mesh to represent the breast surface in 3D for further measurement and shape analysis.

2.1 System configuration

By using off-the-shelf high-resolution digital cameras, high-resolution images achieved to resolve local details of linear densities exceeding 0.1 mm/pixel. There was enough skin texture information of the breast to achieve reliable point-wise correspondences [24, 25]. The photogrammetry system was configured with four stereo-pairs of high resolution cameras to capture the entire breast surface. A camera stereo-pair comprised two cameras (the left camera and the right camera). The stereo-pair captured left and right images. Four

stereo-pairs captured stereo images of the breast from the front, floor and left and right sides; simultaneously in less than $1ms$. The patients were asked to lean over a self-designed posing frame to open the infra mammary fold in order to expose the entire area of each breast for the image capture [26].

2.2 Camera calibration

Photogrammetry obtains 3D coordinates of object points in the 3D space. The 3D coordinates are calculated from the corresponding image co-ordinates from the stereo images of the object based on camera parameters. Exterior parameters of a camera defines its locations in space and its orientations. Inner parameters define the focal length of the lens, the image center, the description of lens distortions. Sensor information can be obtained from manufacturer. In the stereo photogrammetry imaging system developed, the exterior and inner parameters were reliably estimated by the camera calibration [24, 25]. A standard bundles adjustment approach [21] was used to calculate these parameters of each camera. The parameters of location and orientations of cameras enabled the 3D coordinates calculated from the four stereo image pairs to be transformed into a common world coordinate system [27]. In the bundle adjustment, supposing n calibration targets $\{\boldsymbol{P}_j : j = 1, 2, \cdots, n\}$ were imaged by m cameras $\{\boldsymbol{C}_i : i = 1, 2, \cdots, m\}$, this would result in $m \times n$ image coordinates $\{\boldsymbol{p}_{ij} : i = 1, 2, \cdots m, j = 1, 2, \cdots, n\}$ in m images. The perspective projection relationships of

$$\begin{aligned}\boldsymbol{P}_j &= [X_j\ Y_j\ Z_j]^T,\ j = 1, 2, \cdots, n.\\ \boldsymbol{p}_{ij} &= [x_{ij}\ y_{ij}]^T,\ i = 1, 2, \cdots, m; j = 1, 2, \cdots, n.\end{aligned}$$

were used to calculate the camera parameters

$$\boldsymbol{C}_i = [\alpha_i\ \beta_i\ \gamma_i\ X_{io}\ Y_{io}\ Z_{io}\ x_{io}\ y_{io}\ f_i\ \mu_i\ \nu_i\ ]^T,\ i = 1, 2, \cdots, m.$$

In the inputs of the calibration, $[X_j\ Y_j\ Z_j]^T$ were the world co-ordinates of the calibration targets $\boldsymbol{P}_j$; and $[x_{ij}\ y_{ij}]^T$ their image co-ordinates $\boldsymbol{p}_{ij}$. In the outputs of the calibration, $[X_{io}\ Y_{io}\ Z_{io}]^T$ were the world co-ordinates of the perspective centre of camera $\boldsymbol{C}_i$; α_i, β_i and γ_i the three Euler angles defining the orientation of camera $\boldsymbol{C}_i$. $[x_{io}\ y_{io}]^T$ were the image co-ordinates of the principal point for camera $\boldsymbol{C}_i$, f_i the focal length of camera $\boldsymbol{C}_i$, μ_i and ν_i the lens distortions of cameras.

2.3 Stereo matching

Fig. 1 A pair of stereo images and matching results

After the capture of stereo images depicting the breast, the area based stereo matching with a multi-resolution strategy [28] was carried out on each stereo-pair to obtain pair-wise correspondences between the stereo images. The pair-wise correspondences were used to calculate the horizontal and vertical disparities between stereo images. A confidence map was generated from the stereo matching. At each pixel (i, j) of the confidence map was the area-based matching correlation score $c(i, j)$ of local corresponding areas $\boldsymbol{I}_L(i, j)$ centered at (i, j) at in the left image and $\boldsymbol{I}_R(i - d_H, j - d_V)$ centered at $(i - d_H, j - d_V)$ in the right image(Figure 1),

$$c(i, j) = \arg \max_{d_H, d_V} (\boldsymbol{I}_L(i, j) \circ \boldsymbol{I}_R(i - d_H, j - d_V)) \tag{1}$$

where $\circ$ denoted the correlation operator, $d_H(i, j)$ and $d_V(i, j)$ the horizontal and vertical disparities respectively.

2.4 Range Image Integration

Using the principle of triangulation, range images from different stereo pairs were computed from the disparities with the camera calibration parameters [21, 27]. In the system, range images were registered and transformed into common world coordinates (X, Y, Z). The range image was defined in a form

of $\boldsymbol{r}(i,j)$, in which (i,j) were the coordinates of the range image elements. The (i,j) and its perspective centre defined the orientations of $\boldsymbol{r}$. $|\boldsymbol{r}|$ were the Euclidean distance between the perspective centre of the left camera and the points $\boldsymbol{P}(X,Y,Z)$ on the breast surface. $\boldsymbol{P}$ were calculated from the disparities at (i,j). In the range image (Figure 1), the darker pixel indicated the closer was the corresponding 3D point to the camera. In this paper, the main issue of range image integration was addressed in next sections. The integration was affected by the effects of the depth discontinuity.

2.5 The Effects of the Depth Discontinuity

Fig. 2 The examples of mesh constructed from individual range images

The marching cube algorithm was used to integrate multi-view range images into a watertight surface [29]. The marching cubes divided the 3D space of the breast into individual cubes. Supposing a human was viewing the breast from a camera position, the cubes could be classified as *visible* if the cube were in front of the breast surface; *invisible* if the cubes were behind the breast surface. If the breast surface intersected a cube, the cube would be classified as *on surface*. A triangular mesh of the breast would be extracted

from the *on surface* cubes. The resolution of the mesh depended on the size of the marching cubes. Matching cube of 0.5mm size was used for breast surface extraction. Due to self-occlusion, area based stereo matching resulted in depth discontinuity regions in the individual range images. In Figure 2, the surface regions of A, B and C could not be correctly obtained from the stereo images due to the object self-occlusion that depth discontinuities appeared in the mesh. The depth discontinuities have dented the range images, led to some cubes being wrongly classified; resulting in dents in the integrated mesh.

Fig. 3 Artifacts due to depth discontinuities. O_A and O_B are the perspective centers of the left cameras. (k, l) and (m, n) are pixel coordinates in the range images

Further, suppose there were two range images $\boldsymbol{A}$ and $\boldsymbol{B}$ to be merged, the range image $\boldsymbol{B}$ had dented data in the shadowed area (Figure 3) and the range image $\boldsymbol{A}$ also had dented data in the grey area. The dented range data would result in incorrect classifications of the marching cubes in the shadow and grey regions due to ambiguity in selecting correct surfaces in the classification.

Selecting the furthest surface as the valid surface would result in selecting the range data $\boldsymbol{B}$, in the shadow region which would be *wrong* for the integrated surface. The integrated surface had dented regions due to the dented range data of $\boldsymbol{B}$. Selecting the nearest surface as the valid surface will select the range data $\boldsymbol{A}$ in the shadowed region. While this is correct, this results in the other parts of the surface being classified incorrectly, as in the gray region. To overcome the arisen problem due to the depth discontinuities, a progressive reconstruction approach was proposed.

2.6 The Elastic Approach

The progressive approach comprised three major steps:

– Using the marching cubes algorithm [29] to obtain an initial watertight mesh model from multi-view range images.

– Identifying reliable range data representing the valid object surface by decomposing range images to subset patches then removing inaccurate range patches based on the surface normals of the patches.
– Iteratively correcting the initial model elastically based on remaining valid range patches.

2.6.1 Range Image Decomposition

The range image decomposition process made use of range images (Figure 4). A range image was decomposed into *visible*, *invisible*, *overlapping* and *unprocessed* patches, when compared with another range image, for example (Figure 3), range image $\boldsymbol{r}_A(i,j)$ compared with another range image $\boldsymbol{r}_B(i,j)$.

Fig. 4 Range images calculated from recovered disparities

An element (k,l) in the range image $\boldsymbol{r}_A$ (Figure 3) was labeled as *visible*, *invisible*, *overlapping* or *unprocessed* when comparing the range image $\boldsymbol{r}_A$ to the range image $\boldsymbol{r}_B$. A 3-D point $\boldsymbol{P}_A(X,Y,Z)$ on the surface A can be derived from the range data $\boldsymbol{r}_A(k,l)$ at the element of (k,l). The corresponding element (m,n) of the point $\boldsymbol{P}_A(X,Y,Z)$ in the range image $\boldsymbol{r}_B$ was found. At the element (m,n), a range value $|\boldsymbol{r}_B(m,n)|$ was found from the range image $\boldsymbol{r}_B$. Now the element (k,l) at the range image image $\boldsymbol{r}_A$ was labeled as,

$$
\begin{array}{ll}
\textit{visible} & \text{if } |\boldsymbol{r}_B(m,n)| < (\textit{distance of point } O_B \textit{ to point } P_A) - \epsilon \\
\textit{invisible} & \text{if } |\boldsymbol{r}_B(m,n)| > (\textit{distance of point } O_B \textit{ to point } P_A) + \epsilon \\
\textit{overlapping} & \text{if } |\boldsymbol{r}_B(m,n)| - (\textit{distance of point } O_B \textit{ to point } P_A) \leq \epsilon \\
\textit{unprocessed} & \text{if } (m,n) \text{ is out of the range image} \boldsymbol{r}_B
\end{array}
$$

where ϵ was related to the measurement uncertainty, for the system used, $\epsilon = 0.5mm$. When all elements in the masked range image A have been labeled, adjacent elements of the same labels are grouped as *visible*, *invisible*, *overlapping* and *unprocessed* patches.

2.6.2 Removal of Dented Patches

The dented surfaces were caused by the depth discontinuities; and the dented surface normals were nearly perpendicular to the orientation of the camera. The patches with larger view angles from the decomposed range images would be removed. The surface normals of individual patches were calculated to find out the orientation of the patches. At first the points $\boldsymbol{P}_i$ in an individual patch Ω were extracted from the range image. The geometric center $\boldsymbol{P}_c$ of the individual patch was calculated;

$$\boldsymbol{P}_c = \frac{1}{k} \sum_{i \in \Omega} \boldsymbol{P}_i \tag{2}$$

where k is the number of points in the patch. Points in the patch within a neighborhood N of $\boldsymbol{P}_c$ were selected to calculate the covariance matrix $\mathbf{C}$;

$$\mathbf{C} = \frac{1}{n} \sum_{i \in N; N \in \Omega} (\boldsymbol{P}_i - \boldsymbol{P}_c) \cdot (\boldsymbol{P}_i - \boldsymbol{P}_c)^T \tag{3}$$

where n was the number of points in the patch and in the neighborhood of 5mm of centre P_c. The surface normal direction was the least significant eigen vector of the covariance matrix $\mathbf{C}$. If the surface normal direction was nearly perpendicular to the orientation of the camera, the patch was removed from the range image. A threshold of 60 degree was used.

2.6.3 Elastically Repair

After dented range data removal, there were gaps and holes in the range images. It was made use of that the initial mesh $\bar{\boldsymbol{S}}$ obtained from the marching cube algorithm which consisted of valid surfaces and dented regions; and the initial mesh was repaired towards the valid range data to generate a watertight breast mesh. To repair $\bar{\boldsymbol{S}}$ the initial surface model, an elastic deformable model was applied to deform the $\bar{\boldsymbol{S}}$ to a new $\boldsymbol{S}$. The deformation guided by the identified valid range patches $\boldsymbol{r}$ was optimized by minimizing the global energy of the surface:

$$E(\boldsymbol{S}, \bar{\boldsymbol{S}}, r) = E_{ext}(\boldsymbol{S}, r) + \rho E_{int}(\boldsymbol{S}, \bar{\boldsymbol{S}}) \tag{4}$$

in which ρ balanced the internal and external constraints. The external energy term E_{ext} deformed the surface to their most similar valid range data, was defined as:

$$E_{ext}(\boldsymbol{S}, r) = \sum_{i=1}^{n} \omega_i k_{ext} \|\tilde{\boldsymbol{v}}_{\boldsymbol{i}} - \boldsymbol{v}_{\boldsymbol{i}}\|^2 \tag{5}$$

in which n was the number of vertices of the surface; k_{ext} an external elastic modulus; $\tilde{\boldsymbol{v}}_{\boldsymbol{i}}$ the closest point on the valid range patches to the $\boldsymbol{v}_{\boldsymbol{i}}$ the ith vertex of $\boldsymbol{S}$; w_i the similarity between local surface patches at $\boldsymbol{v}_{\boldsymbol{i}}$ and $\tilde{\boldsymbol{v}}_{\boldsymbol{i}}$. The

internal energy term limited the surface deformation to maintain the original surface topology:

$$E_{int}(\boldsymbol{S}, \bar{\boldsymbol{S}}) = \sum_{i=1}^{n} \sum_{j=1\&j\neq i}^{n} k_{int} \|(\boldsymbol{v_i} - \boldsymbol{v_j}) - (\bar{\boldsymbol{v}}_{\boldsymbol{i}} - \bar{\boldsymbol{v}}_{\boldsymbol{j}})\|^2 \tag{6}$$

in which $\boldsymbol{v_i}$ and $\boldsymbol{v_j}$ were edge vertices of $\boldsymbol{S}$; $\bar{\boldsymbol{v}}_{\boldsymbol{i}}$ and $\bar{\boldsymbol{v}}_{\boldsymbol{j}}$ their original positions in $\bar{\boldsymbol{S}}$, k_{int} an internal elastic modulus. Because the energy function was quadratic with respect to $\boldsymbol{v_i}$, the optimization was reduced to a solution of a sparse system of linear equations to be efficiently solved using the conjugate gradient method. The process of optimization was iterative and ended when the distances between $\boldsymbol{v_i}$ and $\tilde{\boldsymbol{v}}_{\boldsymbol{i}}$ were not decreasing any further. In each local optimized deformation, each vertex in the surface found its plausible point on the valid range patches. If the plausible point found, the vertex was labeled as TRUE. The progressive correction algorithm was in the following steps:

1. To identify the plausible points on the valid range data for the vertices $\boldsymbol{v_i}$ of the surface; labeled the vertex with TRUE if it found its plausible point; calculated its displacement $(\tilde{\boldsymbol{v}}_{\boldsymbol{i}} - \boldsymbol{v_i})$, labeled the vertex with FALSE otherwise.
2. To deform neighbor vertices
   a. Started with any vertex labeled with FALSE.
   b. Identified its neighbors of one edge connections in the mesh.
   c. If any of its neighbors were labeled with TRUE, deformed the vertex using the displacement interpolated from the displacements of its neighbors labeled as TRUE, and labeled itself with TRUE; otherwise, went back to the step "a" and found another vertex.
   d. Iteratively repeated the "a" to "c", ended the process if no vertex labeled with FALSE.
3. To calculate the optimal positions of all deformed vertices $\boldsymbol{v_i}$ by minimising the energy of equation (Eq 4, 5, 6).
4. To iteratively repeat 2 to 4. Ended the process if there was no change in differences between $\boldsymbol{v_i}$ and its most similar valid point on $\tilde{\boldsymbol{v}}_{\boldsymbol{i}}$.

2.7 Comparison of Measurements

Nine plaster breast models which represented the human breast in different shapes and sizes were made of polysiloxane condensation-type elastomer and the models were manually textured and painted in a flesh colour [30]. The volumes of the plaster models were measured using the multi-view stereo photogrammetry system. The volume of the plaster models also were measured using the water displacement method [7] which was regarding as a gold standard. The water displacement was conducted by use of a scientific scale that was leveled and calibrated. Each plaster model was fully immersed in a water bowel with full water. The difference in weight of the water content before and after overflow was considered to be equal to the volume of the plaster

model. The volume measurements of the 3D imaging and that of the water displacement method were compared.

3 Results

The calibration error was checked by projecting the physical calibration target back to its image plane. Comparing the differences between the image of the calibration target and the back projected target image, the calibration errors were found between 0.2 to 0.5 pixel. Verified by comparing a surface profile with the measurement of a titled flat surface [25], the depth measurement error was found less than 0.5mm.

The purpose of the range image decomposition was to remove dented range data from the range images before the elastic modeling. The decomposition has been tested with view angle thresholds from 40 to 70 degrees and the ϵ values from 0 to 1.5mm which define the overlapping regions. Figure 5 displayed one of the range images which has been decomposed based on different ϵ values and thresholded with different angles where the visible regions were bright, invisible regions gray, overlapping zones dark and removed regions black.

Fig. 5 Decomposed Regions of Range images with thresholding angles of 40 to 70 degree and overlapping tolerance from 0 to 1.5mm

The value of ϵ defined the overlapping regions. The smaller the value was, the finer was the overlapping zones. When the value of ϵ was set to zero, ultimately there are only visible and invisible regions in the decomposed range images. The thresholding view angle has a more significant effect on the dented range data removal. The smaller the thresholding angle was, the more range data were removed. The decomposition process has been applied on 15 cases of objects of face, breast and pig. With the value of ϵ was set to 0.1mm and the thresholding angle to 60 degree, their dented range data have been removed for all 15 cases.

The range images of four views were calculated and integrated using the marching cube algorithm to obtain a single watertight breast surface (Figure

6). Elastic modelling has been applied for the dented range data removal to reconstruct a correct breast surface for volume measurement (Figure 7).

Fig. 6 One breast surface reconstructed from the mult-view range images

Fig. 7 The correct breast surface after elastic modelling

The volume measurements of the water displacement and that of the 3D imaging were shown in the table 1. The mean difference between the volume measurements of the 3D imaging and that of the water displacement was 11.12cc with STD 23.23cc, SEM 7.74cc. The Minimal Detectable Change(MDC) was calculated in terms of 95% confidence, which was 21.85cc. Interclass correlation cofficient (ICC) was 0.9945. A paired student t-test was carried out. The probability p = 0.1888 with t=1.4365 and student threshold

3.355. Because of p >0.1, the mean difference of the two volumes 11.22cc with STD 23.23cc, did not differ significantly from zero.

Table 1 The volume measurements of the water displacement and 3D imaging

Plaster Model	Water dis. (cc)	3D imaging (cc)	difference(cc)
1	364.60	354.40	-10.20
2	434.70	422.30	-12.40
3	579.00	613.40	34.40
4	231.10	209.50	-21.60
5	433.40	465.10	31.70
6	591.60	610.50	18.90
7	596.60	620.70	24.10
8	100.40	96.10	-4.30
9	863.10	902.60	39.50
	Paired t-test: p=0.1888 >0.1		
	Intraclass correlation: ICC = 0.9945		

4 Discussion

Each different system has advantages and disadvantages, indications and restriction as well as different needs for environments and costs attached. The 3D stereophotogrammetry image system developed provided an alternative option for data collection and evaluation. It offered a convenient approach to measure the shapes of breasts, which had advantages over structured light projection [10, 11], the laser scanning [4, 12, 13, 14] in terms of the capturing time (less than 1ms), the photographic skin texture; and over 3D X-ray imaging [18, 19, 20] in terms of the radiation free nature. The photographic skin texture was important for the clinicians to identify the anatomical landmarks. In the clinical research, it was constrained with resources that it would not be able to compare the measurements with that of the structured light project, laser scanning and X-Ray/MRI.

Multi-view stereophotogrammetry imaging system offered a chance for the patients to open up the infra mammary fold and expose the entire area of each breast for fast image captures. Using multi-view stereo imaging photogrammetry, multi-view range images had to be integrated into a single mesh for the breast volume measurements. There were four major approaches of multi-view range image integration: point based methods, direct range zipping, volumetric approaches employing implicit surfaces and model based methods. Point based methods [31, 32] directly integrated surfaces from points of multi-view range data, however the method of directly integrating surface from range data points would result in poor 3D quality because of range data noise and registration errors. Furthermore the point based methods did not made use of the connections of points in range images. In direct range zipping approaches [33] identification of overlapping surface areas between range images was needed. Wang and Oliveira [34] applied a Moving Least Squares algorithm. Zhou and

Liu [35] improved the accuracy of detection of overlapping areas by applying k-means clustering. Direct range zipping approaches had difficulties of filling convoluted holes [36]. The detection of overlapping areas and removing inaccurate range data was crucial for these approaches while it was lack of details of how inaccurate range data were removed. Volumetric approaches [37, 38] were applied to construct watertight, non-redundant surfaces, but these approaches were sensitive to depth discontinuities which would lead to a less plausible surface. Model based approaches [39, 40, 41] might offer a solution to overcome the depth discontinuity problem, but it was unavoidable prerequisite to formulate a model of the object to be reconstructed. In the current study, an progressive approach was proposed, similar to the model based approaches; the model was generated by the system itself and used as the initial model to improve the quality of the multi-view range image integration. The breast volume measurements of the developed system has been compared with that of the water displacement [30].

Further research is required to identify the self-occlusion regions in the stereo matching stage automatically and precisely that the dented range data would be removed before integrating the multi-view range images. The multi-view range image integration would be not affected by the ambiguity caused by the depth discontinuities. In the table 1, large breasts were overestimated whereas small breasts were underestimated. It was due to the software developed for measuring breast volume from 3D breast meshes. A chest wall had to be formed from breast's boundary in order to measure the volume. The way to form the chest wall affected the measurements. Further investigations are required. Based on the advantages of the work, further shape analysis will be applied on the beauty factors of the breasts.

5 Conclusion

In this paper, a 3D multi-view stereophotogrammetry system for the breast volume measurement was presented. The quality of range image integration has been improved by removing the inaccurate range data and the iterative elastic modelling was used to integrate the range images of four views into a watertight mesh for breast volume measurement. With statistical analysis results of the mean difference, the minimal detectable change and the interclass correlation coefficient, it was concluded that the 3D stereophotogrammetry image system developed was more reliable than the method of water displacement.

6 Compliance with Ethical Standards

The source of data is 3D stereophotogrammetry images of the breast following cancer resection and reconstruction.

Conflict of interest: The authors declare that they have no conflict of interest.

Ethical Approval: All procedures performed in studies involving human participants were in accordance with the ethical standards of the institutional and/or national research committee and with the 1964 Helsinki declaration and its later amendments or comparable ethical standards. Approval has been granted form national ethics committee (IRAS) and sponsorship was obtained from Greater Glasgow & Clyde Health Board (R & D Ref: WN08BU237) of the UK.

Informed consent: Informed consent was obtained from all individual participants included in the study.

References

1. U. Mahmood, A. Hanlon, M. Koshy, R. Buras, S. Chumsri, K. Tkaczuk, S. Cheston, W. Regine, and S. Feigenberg, "Increasing national mastectomy rates for the treatment of early stage breast cancer," *Annals of Surgical Oncology*, vol. 20, no. 5, pp. 1436–1443, 2013.
2. J. Lee, M. Kawale, F. A. Merchant, J. Weston, M. C. Fingeret, D. Ladewig, G. P. Reece, M. A. Crosby, E. K. Beahm, and M. K. Markey, "Validation of stereophotogrammetry of the human torso," *Breast Cancer (Auckl).*, vol. 5, pp. 15–25, 2011.
3. M. Kim, J. Sbalchiero, G. Reece, M. Miller, E. Beahm, and M. Markey, "Assessment of breast aesthetics," *Plast Reconstr Surg.*, vol. 121(4), pp. 186–194, 2008 April.
4. O. M. Tepper, N. S. Karp, K. Small, J. Unger, L. Rudolph, A. Pritchard, and M. Choi, "Three-dimensional imaging provides valuable clinical data to aid in unilateral tissue expander-implant breast reconstruction.," *Breast J*, vol. 14, no. 6, pp. 543–550, 2008.
5. J. Georgii, M. Eder, K. Burger, S. Klotz, F. Ferstl, L. Kovacs, and R. Westermann, "A computational tool for pre-operative breast augmentation planning in aesthetic plastic surgery.," *IEEE J Biomed Health Inform*, Oct 2013.
6. L. J. Sigurdson and S. A. Kirkland, "Breast volume determination in breast hypertrophy: an accurate method using two anthropomorphic measurements," *Plastic & Reconstructive Surgery*, vol. 118(2), pp. 313–320, 2006.
7. D. Milligan, J. Drife, and S. R, "Changes in breast volume during normal menstrual cycle and after oral contraceptives," *Br Med J*, vol. 29(4), pp. 494–496, 1975.
8. J. Fleming, T. Hames, and J. Smallwood, "Comparison of volume changes in the forearm assessed by impedance and water-displacement plethysmography," *Medical and Biological Engineering and Computing*, vol. 24, no. 4, pp. 375–378, 1986.
9. A. Edsander-Nord, M. Wickman, and G. Jurell, "Measurement of breast volume with thermoplastic casts," *Scand J Plast Reconstr Hand Surg*, vol. 30, pp. 129–132, 1996.
10. A. Ishida, Y. Mori, H. Kishimoto, T. Nakazima, and H. Tsubakimoto, "Body shape measurement for scoliosis evaluation," *Medical and Biological Engineering and Computing*, vol. 25, no. 5, pp. 583–585, 1987.
11. V. Pazos, F. Cheriet, L. Song, H. Labelle, and J. Dansereau, "Accuracy assessment of human trunk surface 3d reconstructions from an optical digitising system," *Medical and Biological Engineering and Computing*, vol. 43, no. 1, pp. 11–15, 2005.
12. D. Esme, A. Bucksch, and W. Beekman, "Three-dimensional laser imaging as a valuable tool for specifying changes in breast shape after augmentation mammaplasty," *Aesthetic Plastic Surgery*, vol. 33, pp. 191–195, 2009.
13. B. J. DuBray Jr, R. V. Levy, P. Balachandran, K. D. Conzen, G. A. Upadhya, C. D. Anderson, and W. C. Chapman, "Novel three-dimensional imaging technique improves the accuracy of hepatic volumetric assessment," *HPB*, vol. 13, no. 9, pp. 670–674, 2011.
14. U. Ahcan, D. Bracun, K. Zivec, R. Pavlic, and P. Butala, "The use of 3d laser imaging and a new breast replica cast as a method to optimize autologous breast reconstruction after mastectomy," *The Breast*, 2011.
15. C. W. Loughry, D. B. Sheffer, T. E. Price, M. J. Lackney, R. G. Bartfai, and W. M. Morek, "Breast volume measurement of 248 women using biostereometric analysis.," *Plastic and Reconstructive Surgery*, vol. 80, no. 4, pp. 553–558, 1987.

16. C. Malata, J. Boot, E. Bradbury, A. Ramli, and D. Sharpe, "Congenital breast asymmetry: subjective and objective assessment," *British Journal of Plastic Surgery*, vol. 47, no. 2, pp. 95 – 102, 1994.
17. C. S. Sun, M. K. Markey, F. A. Merchant, K. Ravi-Chandar, M. C. Fingeret, and G. P. Reece, "3d computer technology addresses body-image issues of breast reconstruction," *SPIE Newsroom. DOI: 10.1117/2.1201307.005016*, 25 July 2013.
18. R. Benjamin, S. Prakoonwit, I. Matalas, and R. Kitney, "Object-based three-dimensional x-ray imaging," *Medical and Biological Engineering and Computing*, vol. 34, no. 6, pp. 423–430, 1996.
19. A. Mitulescu, I. Semaan, J. De Guise, P. Leborgne, C. Adamsbaum, and W. Skalli, "Validation of the non-stereo corresponding points stereoradiographic 3d reconstruction technique," *Medical and Biological Engineering and Computing*, vol. 39, no. 2, pp. 152–158, 2001.
20. R. Dumas, B. Blanchard, R. Carlier, C. de Loubresse, J.-C. Le Huec, C. Marty, M. Moinard, and J.-M. Vital, "A semi-automated method using interpolation and optimisation for the 3d reconstruction of the spine from bi-planar radiography: a precision and accuracy study," *Medical & Biological Engineering & Computing*, vol. 46, no. 1, pp. 85–92, 2008.
21. C. C. Slama, ed., *Manual of Photogrammetry*. 5410 Grosvenor Lane, Suite 210, Bethesda, MD 20814-2160, USA.: American Society for Photogrammetry and Remote Sen, 1980.
22. R. Tsai, "A versatile camera calibration technique for high-accuracy 3d machine vision metrology using off-the-shelf tv cameras and lenses," *IEEE JOURNAL OF ROBOTICS AND AUTOMATION*, vol. 3, pp. 323–344, Aug. 1987.
23. Z. Zhang, "A flexible new technique for camera calibration," *IEEE Transactions on Pattern Analysis and Machine Intelligence*, vol. 22, pp. 1330–1334, Nov. 2000.
24. X. Ju, P. Siebert, N. McFarlane, J. Wu, R. Tillett, and P. Schofield, "A stereo imaging system for the metric 3d recovery of porcine surface anatomy," *Sensor Review*, vol. 24(3), pp. 298–307, 2004.
25. J. Wu, R. Tillett, N. McFarlane, X. Ju, P. Siebert, and P. Schofield., "Extracting the three-dimensional shape of live pigs using stereo photogrammetry," *Computers and Electronics in Agriculture*, vol. 44, pp. 203–222, 2004.
26. H. Henseler, X. Ju, A. Ayoub, and A. K. Ray, "The importance of the pose in three-dimensional imaging of the ptotic breast.," *J Plast Reconstr Aesthet Surg*, vol. 66, pp. 1551–1556, Nov 2013.
27. C. W. Urquhart, "The active stereo probe: The design and implementation of an active videometrics system. phd thesis.," tech. rep., University of Glasgow, 1997.
28. J. P. Siebert and C. W. Urquhart, "C3d: a novel vision-based 3d data acquisition system," in *Proceedings of the Mona Lisa European Workshop, Combined Real and Synthetic Image Processing for Broadcast and Video Production*, (Hamburg, Germany), August 1998.
29. W. E. Lorensen and H. E. Cline, "Marching cubes: A high resolution 3d surface construction algorithm," *ACM SIGGRAPH Computer Graphics*, vol. 21(4), pp. 163–169, 1987.
30. H. Henseler, B. S. Khambay, A. Bowman, J. Smith, J. P. Siebert, S. Oehlera, X. Ju, A. Ayoub, and A. K. Raya, "Investigation into accuracy and reproducibility of a 3d breast imaging system using multiple stereo cameras.," *Journal of Plastic, Reconstructive & Aesthetic Surgery*, vol. 64(5), pp. 577–582, May 2011.
31. T. K. Dey, S. Goswami, and T. Cocone, "A watertight surface reconstructor," *Journal of Computer and Information Science and Engineering*, vol. 13, pp. 302–307, 2003.
32. C. Zhu and W. K. Leow, "Textured mesh surface reconstruction of large buildings with multi-view stereo," *The Visual Computer*, pp. 1–7, 2013.
33. G. Turk and M. Levoy, "Zippered polygon meshes from range images," in *SIGGRAPH94*, July 24-29 1994.
34. J. Wang and M. M. Oliveira, "A hole-filling strategy for reconstruction of smooth surfaces in range images," *Computer Graphics and Image Processing, 2003. SIBGRAPI 2003. XVI Brazilian Symposium on 2003*, pp. 11–18, 2003.
35. H. Zhou and Y. Liu, "Accurate integration of multi-view range images using k-means clustering," *Pattern Recognition*, vol. 41, pp. 151–175, 2008.

36. J. Davis, S. R. Marschner, M. Garr, and M. Levoy, "Filling holes in complex surfaces using volumetric diffusion," in *Proc. First International Symposium on 3D Data Processing Visualization and Transmission*, pp. 428–861, June 19–21, 2002.
37. B. Curless and M. Levoy, "A volumetric method for building complex models from range images," in *SIGGRAPH*, pp. 302–312, 1996.
38. Z. Li, W. Jia, Z.-H. Mao, J. Li, H.-C. Chen, W. Zuo, K. Wang, and M. Sun, "Anthropometric body measurements based on multi-view stereo image reconstruction," in *Engineering in Medicine and Biology Society (EMBC), 2013 35th Annual International Conference of the IEEE*, pp. 366–369, IEEE, 2013.
39. R. Plankers and P. Fua, "Articulated soft objects for multiview shape and motion capture," *PAMI*, vol. 25(9), pp. 1182–1187, 2003.
40. J. Starck and A. Hilton, "Model-based multiple view reconstruction of people," in *ICCV2003*, pp. pp915–922, 2003.
41. E. Jolivet, B. Sandoz, S. Laporte, D. Mitton, and W. Skalli, "Fast 3d reconstruction of the rib cage from biplanar radiographs," *Medical & Biological Engineering & Computing*, vol. 48, no. 8, pp. 821–828, 2010.

Fig1
Click here to download Figure: Fig1.tif

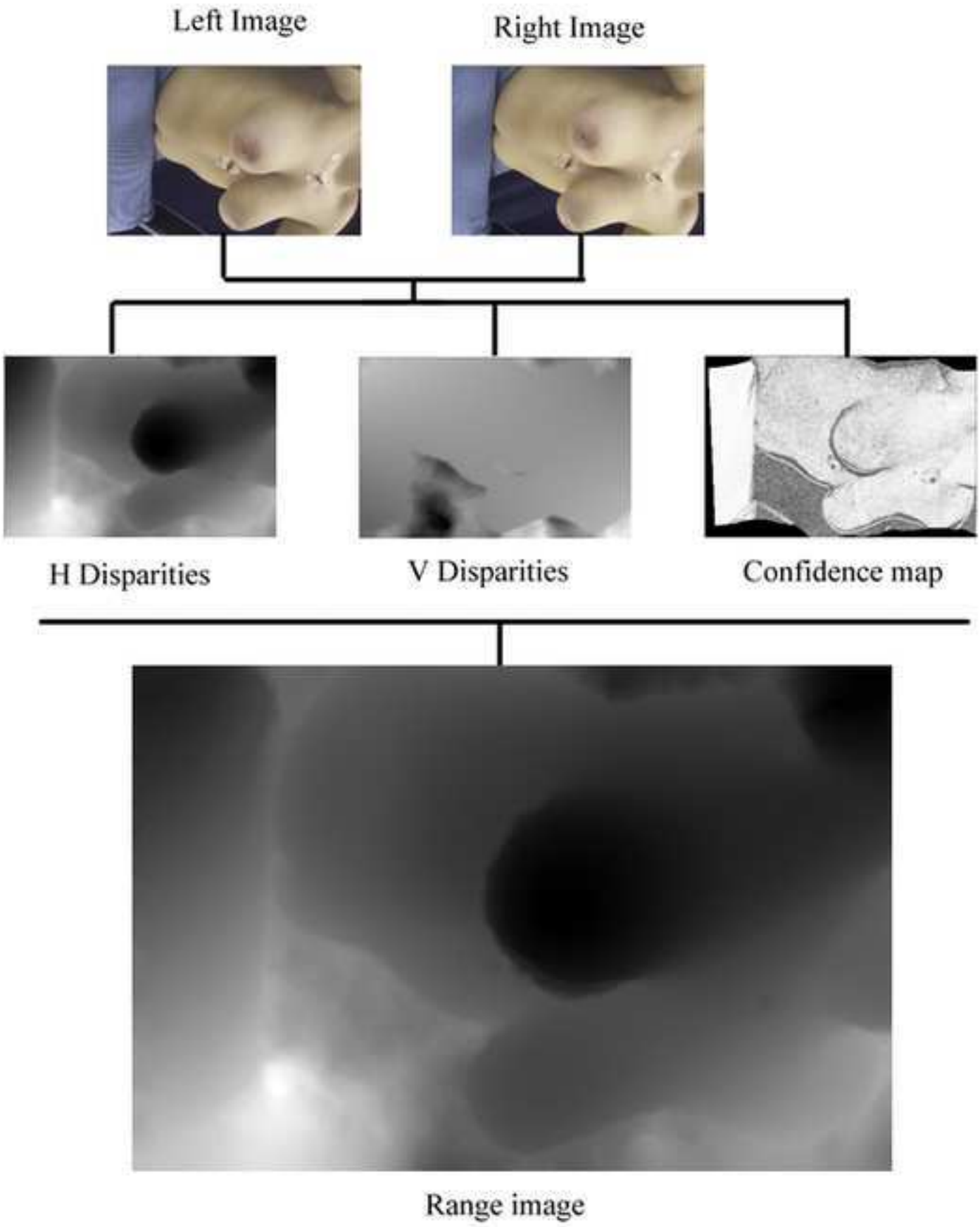

Fig2
Click here to download Figure: Fig2.tif

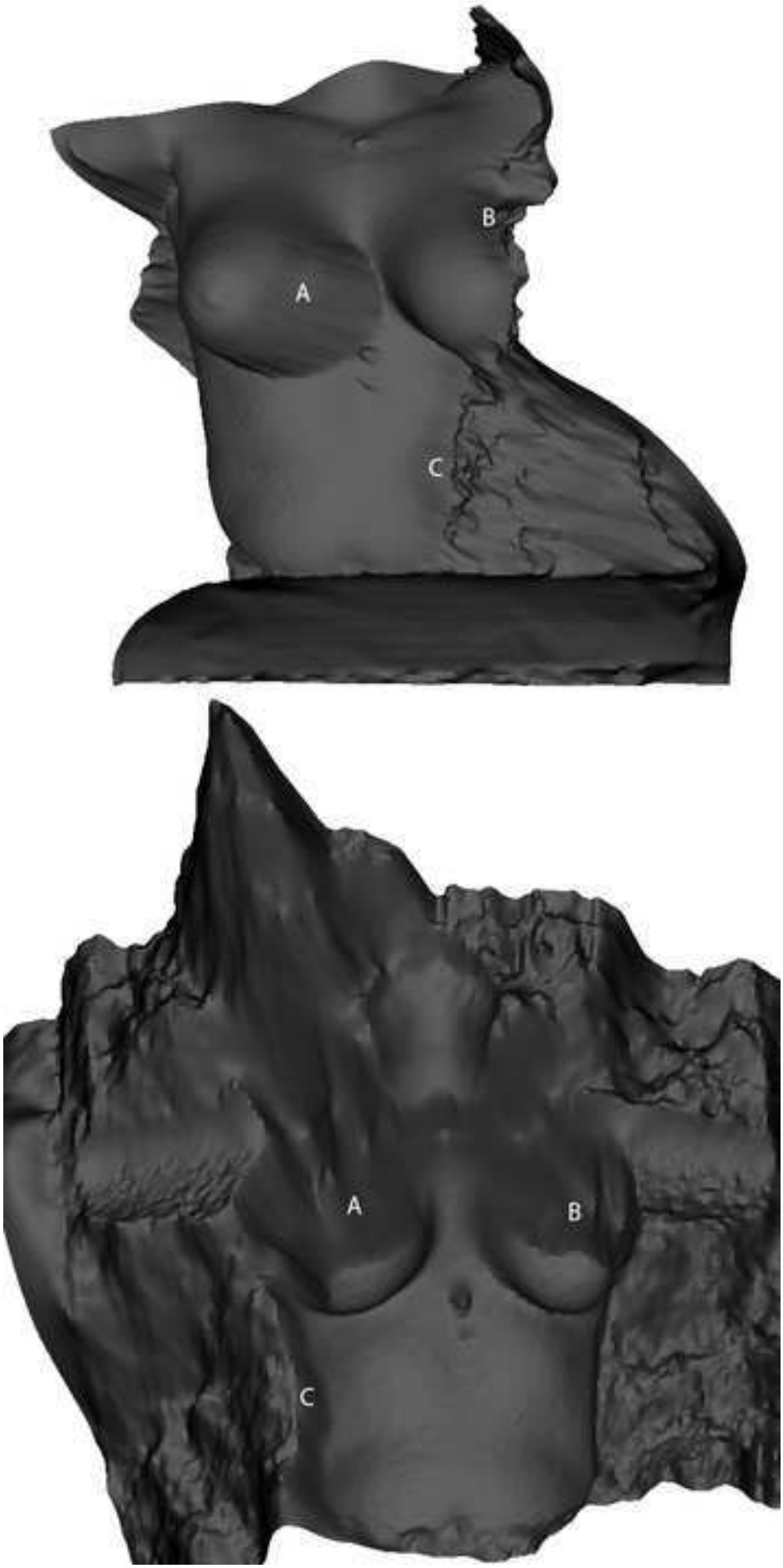

Fig3
Click here to download Figure: Fig3.tif

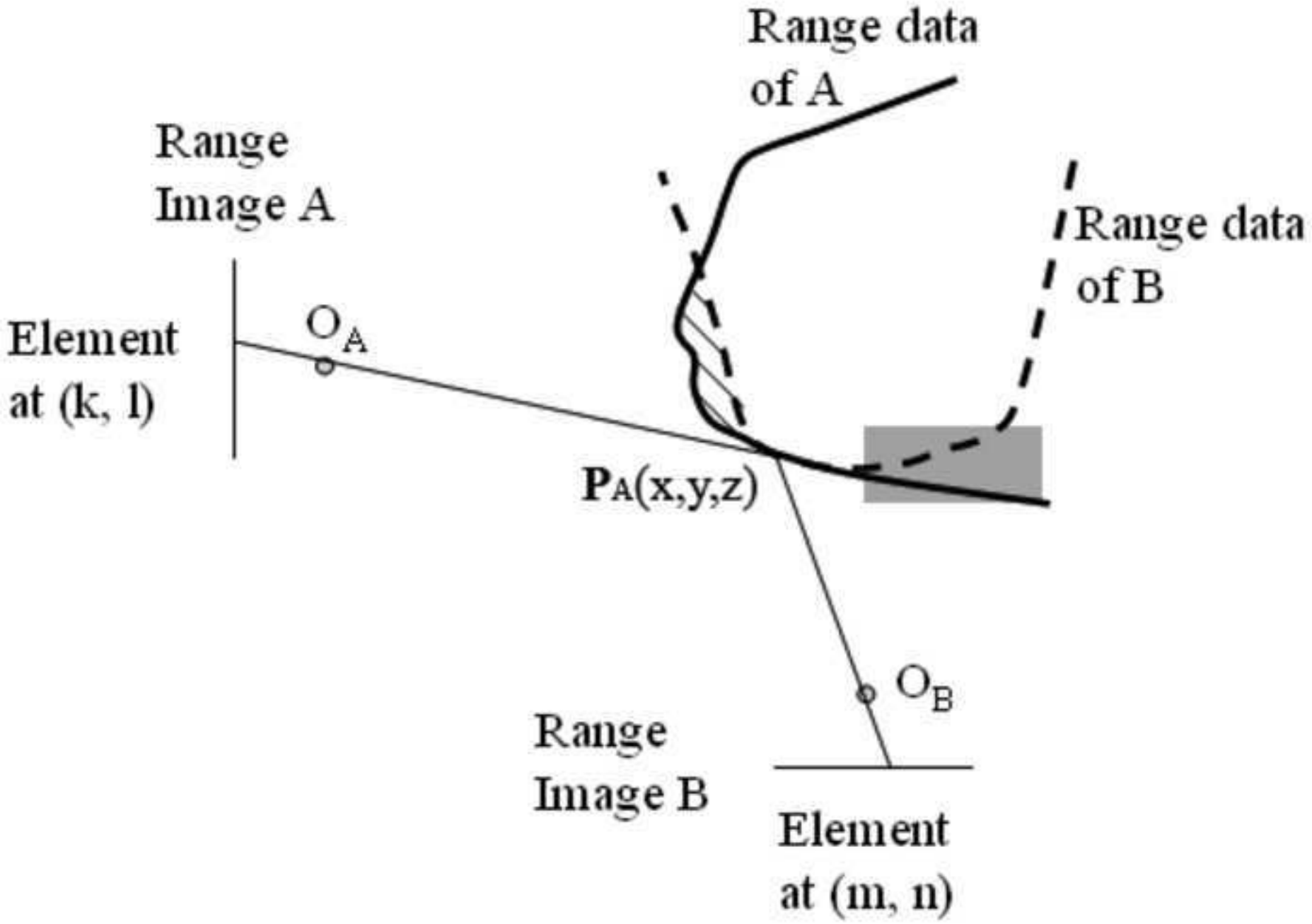

Fig4
Click here to download Figure: Fig4.tif

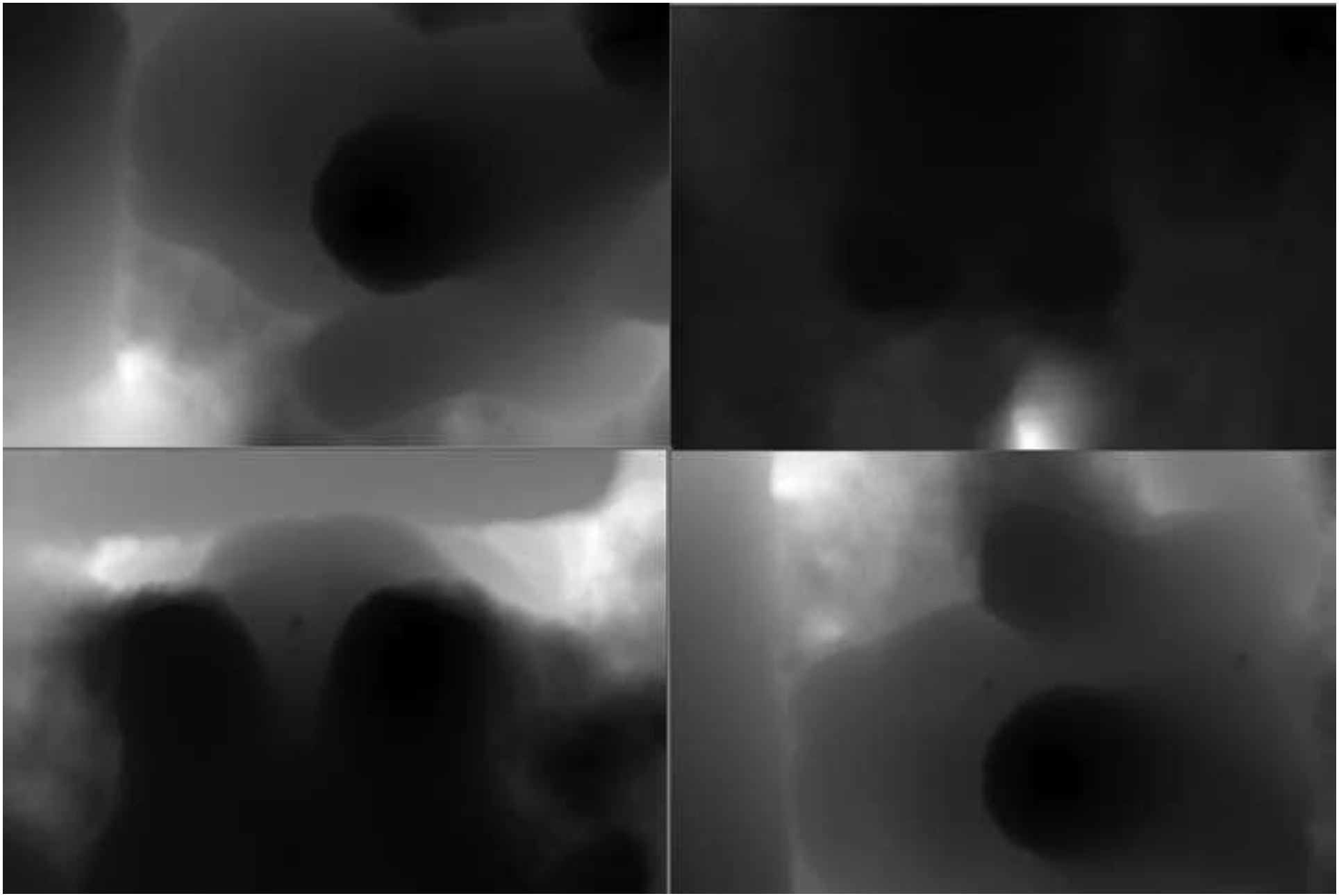

Fig5
Click here to download Figure: Fig5.tif

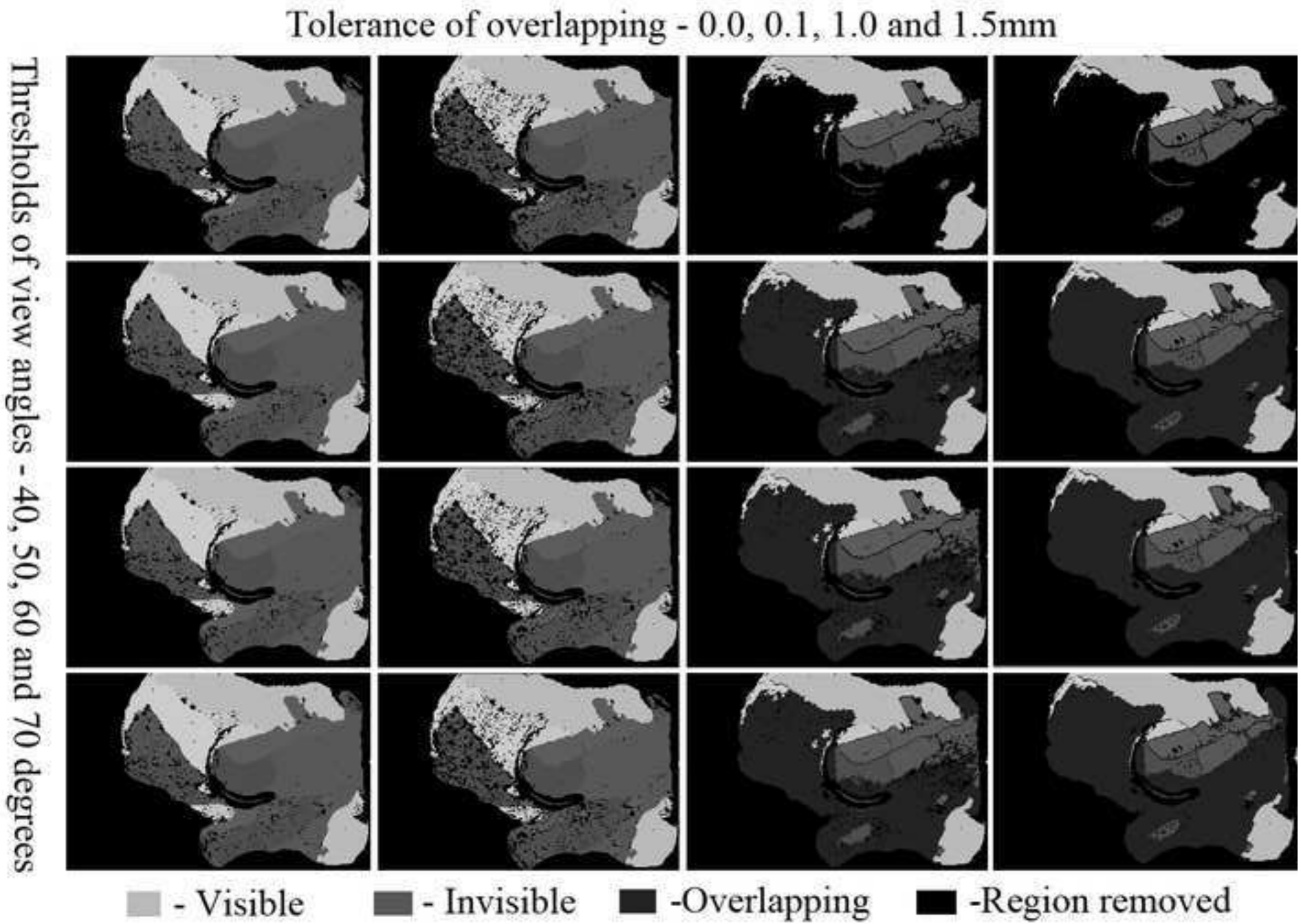

Fig6
Click here to download Figure: Fig6.tif

Fig7
Click here to download Figure: Fig7.tif